methods

Multimodal imaging approach to monitor browning of adipose tissue in vivo[S]

Xin Hui Derryn Chan,* Ghayathri Balasundaram,[1,†] Amalina Binte Ebrahim Attia,[1,†] Julian L. Goggi,[1,§,] Boominathan Ramasamy,[§] Weiping Han,[††] Malini Olivo,[†,§§] and Shigeki Sugii[2,*,***]**

Fat Metabolism and Stem Cell Group,* Laboratory of Bio-Optical Imaging,[†] Isotopic Molecular Imaging Group,[§] and Laboratory of Metabolic Medicine,[††] Singapore Bio-imaging Consortium, Agency for Science, Technology, and Research (A*STAR), Singapore; Department of Physiology,** Yong Loo Lin School of Medicine, National University of Singapore, Singapore; School of Physics,[§§] National University of Ireland Galway, Galway, Ireland; and Cardiovascular and Metabolic Disorders Program,*** Duke-National University of Singapore Medical School, Singapore

Abstract The discovery that white adipocytes can undergo a browning process to become metabolically active beige cells has attracted significant interest in the fight against obesity. However, the study of adipose browning has been impeded by a lack of imaging tools that allow longitudinal and noninvasive monitoring of this process in vivo. Here, we report a preclinical imaging approach to detect development of beige adipocytes during adrenergic stimulation. In this approach, we expressed near-infrared fluorescent protein, iRFP720, driven under an uncoupling protein-1 (*Ucp1*) promoter in mice by viral transduction, and used multispectral optoacoustic imaging technology with ultrasound tomography (MSOT-US) to assess adipose beiging during adrenergic stimulation. We observed increased photoacoustic signal at 720 nm, coupled with attenuated lipid signals in stimulated animals. As a proof of concept, we validated our approach against hybrid positron emission tomography combined with magnetic resonance (PET/MR) imaging modality, and quantified the extent of adipose browning by MRI-guided segmentation of 2-deoxy-2-^{18}F-fluoro-D-glucose uptake signals. The browning extent detected by MSOT-US and PET/MR are well correlated with *Ucp1* induction.[jlr] Taken together, these systems offer great opportunities for preclinical screening aimed at identifying compounds that promote adipose browning and translation of these discoveries into clinical studies of humans.—Chan, X. H. D., G. Balasundaram, A. B. E. Attia, J. L. Goggi, B. Ramasamy, W. Han, M. Olivo, and S. Sugii. **Multimodal imaging approach to monitor browning of adipose tissue in vivo. *J. Lipid Res.* 2018.** 59: **1071–1078.**

Supplementary key words adipocytes/obesity • beige fat • bio-optical imaging • diabetes • lipids • metabolic disease • molecular imaging • photoacoustic imaging • uncoupling protein-1

The increasing prevalence of obesity in developed countries is driving research into metabolic diseases, particularly obesity and its associated complications. Metabolically active brown adipose tissue (BAT) in adult humans was identified through improved imaging with positron emission tomography combined with computed tomography (PET/CT) (1–5). This has led to a paradigm shift in metabolic disease investigations and intensified the scrutiny of BAT as a systemic energy regulator. Studies have demonstrated that the amount of BAT found in adult humans is inversely correlated with body mass index, with the lowest found in obese individuals (5, 6); therefore, increasing BAT mass has been proposed as a potential therapy against obesity. Unlike white adipocytes, which are responsible for energy storage, brown adipocytes are responsible for dissipating chemical energy in the form of heat mediated by the function of uncoupling protein-1 (UCP1). UCP1 is responsible for reducing the membrane potential and thereby uncoupling oxidative phosphorylation from ATP synthesis, burning glucose and fatty acids, leading to improved glucose homeostasis and blood lipid profiles (7, 8). BAT in humans, similar to BAT in rodents, was recently shown

This work was supported by intramural funding from the Biomedical Research Council, Agency for Science, Technology and Research, Singapore.

Manuscript received 11 January 2018 and in revised form 13 March 2018.

Published, JLR Papers in Press, April 13, 2018
DOI https://doi.org/10.1194/jlr.D083410

Abbreviations: AAV, adeno-associated virus; au, arbitrary unit; BAT, brown adipose tissue; ^{18}F-FDG, 2-deoxy-2-^{18}F-fluoro-D-glucose; FSK, forskolin; iRFP, infrared fluorescent protein; ID, injected dose; iWAT, inguinal WAT; MSOT-US, multispectral optoacoustic imaging technology with ultrasound tomography; PET/CT, positron emission tomography combined with computed tomography; PET/MR, positron emission tomography combined with magnetic resonance; PGK, phosphoglycerate kinase; rAAV, recombinant adeno-associated virus; UCP1, uncoupling protein-1; WAT, white adipose tissue.

[1] G. Balasundaram, A. B. E. Attia, and J. L. Goggi contributed equally to this work.

[2] To whom correspondence should be addressed.
e-mail: shigeki_sugii@sbic.a-star.edu.sg

[S] The online version of this article (available at http://www.jlr.org) contains a supplement.

to be effectively stimulated by β3-adrenergic receptor agonists (9).

Recent studies have identified two types of thermogenic adipocytes, the classical brown adipocytes and beige adipocytes (10). Beige adipocytes can be found interspersed among the subcutaneous white adipose tissue (WAT) upon "browning" in response to cold exposure or pharmacological stimuli (11–14). Similar to the classical brown adipocytes, beige adipocytes are characterized by multi-locular lipid droplets and express brown fat-specific genes, such as *Ucp1* and *Cidea*. Human BAT is more similar to rodent beige fat than it is to classical rodent inter-scapular BAT in molecular characteristics and signatures (10, 15). Therefore, there is considerable interest in identifying biological mechanisms and new drug molecules capable of stimulating rodent beige fat as a surrogate for human BAT. However, noninvasive preclinical imaging tools that enable longitudinal assessment of biological changes or efficacy of pharmacological interventions for beige adipocyte recruitment are still lacking.

To date, several imaging approaches, such as PET/CT and MRI have attempted to quantify BAT in vivo. Although PET/CT imaging has been instrumental in the identification of BAT in humans and is routinely used in functional characterization of BAT activity in rodents, it necessitates exposure to ionizing radiation and, thus, is not suitable for longitudinal studies where repeated scans are required. On the other hand, MRI has been employed for characterizing BAT independently of its metabolic activity, based on the unique chemical-shift water-fat signals due to differences in morphology and chemical composition between WAT and BAT (16). Despite this development, the reliable localization and quantification of WAT browning can be impeded by its relatively poor resolution and sensitivity, which obfuscate the detection of interspersed beige adipocytes in WAT. To overcome the challenges associated with the aforementioned imaging techniques, positron emission tomography combined with magnetic resonance (PET/MR) hybrid imaging modality has been developed as an alternative to PET/CT, which enables the assessment of radio-labeled tracer 2-deoxy-2-^{18}F-fluoro-D-glucose (^{18}F-FDG) uptake by PET along with the anatomical description measured from MR.

Recent studies have also explored the feasibility of optical imaging for BAT localization, which relatively has ease of use and low cost, making it an attractive modality for preliminary in vivo screening in small animals. Conventional optical imaging techniques, however, are limited by spatial resolution and light scattering in tissues and can be overcome with multispectral optoacoustic imaging technology with ultrasound tomography (MSOT-US) (17, 18). Near-infrared fluorescent protein (iRFP) engineered from bacterial phytochrome photoreceptors was previously shown to be a good optoacoustic contrast agent due to its high extinction coefficients and low fluorescence quantum yields (19). The use of iRFP as a reporter protein coupled with MSOT's newly demonstrated capacity to image reporter proteins in deep tissues opens up the possibility of visualizing dynamic molecular and cellular processes (20–22). Here, we describe an imaging protocol utilizing MSOT-US to monitor endogenous browning of fat sensitively and noninvasively using a near-infrared fluorescent iRFP720 reporter driven by *Ucp1* promoter. Browning of WAT in vivo can then be assessed through longitudinal quantification of near-infrared fluorescent activity as a surrogate marker for *Ucp1* expression. Using a combination of MSOT-US and PET/MR imaging, we demonstrate that iRFP720 signals recapitulate *Ucp1* expression in vivo and are well correlated with ^{18}FDG uptake in WAT during adrenergic stimulation. Collectively, our findings suggest that these imaging platforms can be useful for monitoring and quantifying adipose browning in vivo, as well as providing new insights to the biological processes of beige fat differentiation and regulation.

MATERIALS AND METHODS

Cell culture

The 3T3L1 preadipocytes (ATCC) were cultured on gelatin-coated plates and maintained in DMEM (Invitrogen, Gibco) supplemented with 10% newborn calf serum, and penicillin and streptomycin were added to a final concentration of 100 U/ml. For white adipocyte differentiation, confluent 3T3L1 cells were cultured in DMEM and 10% FBS supplemented with 167 nM insulin, 1 mM dexamethasone, and 0.5 mM isobutylmethylxanthine for 2 days. After 2 days, the cells were maintained in DMEM and 10% FBS supplemented with 167 nM insulin. On day 4, the medium was changed to DMEM containing 10% FBS until harvest. For induction into brown adipocytes, differentiated 3T3L1 cells were treated with 10 mM forskolin (FSK) for 6 h. HEK293T cells were grown and maintained in DMEM supplemented with 10% FBS and 100 U/ml penicillin-streptomycin. Cultures were maintained at 37°C and 5% CO_2.

Plasmid constructs

The following expression constructs were purchased from Addgene: piRFP720-N1 (#45461) and pAAV-MCS2 (#46954). To generate the pAAV-mini/UCP1-iRFP720 reporter construct, the short version of the Ucp1 promoter (mini/Ucp1) and infrared fluorescent protein (iRFP720) reporter were cloned into the pAAV-MCS2 with *Nhe*I and *Nco*I restriction sites at the 5′ and 3′ ends, respectively. To generate the constitutive phosphoglycerate kinase (PGK)-iRFP720 lentiviral construct, iRFP720 reporter was cloned downstream of the PGK promoter in pCDH-PGK-MCS-EF1-GFP vector (a kind gift from Dr. Srikanth Nama) using the *Eco*RI and *Not*I restriction sites at the 5′ and 3′ ends, respectively. PGK promoter in the PGK-iRFP720 construct was replaced with the mini/Ucp1 promoter using the *Cla*I and *Xba*I restriction sites to generate the mini/Ucp1-iRFP720 lentiviral construct.

Lentivirus and adeno-associated virus preparation

Third generation lentivirus was produced by cotransfecting HEK293T cells with 10 μg of transfer vector and three packaging plasmids: 6.5 μg pMDLg/pRRE, 2.5 μg pRSV-REV, and 3.5 μg pMD2.G. Transfection was performed using jetPRIME transfection reagent (Polyplus) as per the manufacturer's protocol. Viral supernatant was collected 48 and 72 h post transfection. Supernatant was purified by filtering through a 0.22 μm low protein binding membrane and concentrated by ultracentrifugation. Viral particles were resuspended in 1× Hanks' balanced salt solution, aliquoted, and stored at −80°C. Virus titers were determined by infecting HEK293T cells with serially diluted virus for 72 h, followed by flow cytometry analysis of GFP expression. Recombinant adeno-associated virus (rAAV) was produced by cotransfecting HEK293T cells with three plasmids: AAV transgene expression plasmid, AAV-2/8 packaging plasmid, and adenoviral helper pF Δ6. The AAV expression plasmid encodes iRFP720 driven by the mini/UCP1 promoter. rAAV was packaged and purified as previously described (23).

Quantitative real-time PCR

Total RNA was extracted with TRIzol (Invitrogen) and then purified using RNeasy (Qiagen) following manufacturer's protocol. Reverse transcription was performed using RevertAid First Strand cDNA synthesis kit (Fermentas). Gene expression was analyzed using Power SYBR Green PCR Master Mix with a StepOne Plus real-time PCR system. Relative gene expression was calculated using the $2^{-\Delta\Delta CT}$ method and normalized to 18S rRNA expression. The primer sequences used can be found in supplemental Table S1.

Western blotting

Tissues were lysed using RIPA buffer with protease and phosphatase inhibitors. Proteins were separated by SDS-PAGE, transferred to nitrocellulose membrane and probed with α tubulin (1:1,000; T5168, Sigma) and UCP1 antibodies (1:1,000; ab23841, Abcam).

Fluorescence microscopy

Following browning induction with 10 mM FSK for 6 h, differentiated adipocytes expressing mini/Ucp1 iRFP720 were imaged using a Nikon A1Rsi$^+$ confocal laser microscope system with a 100× NA/1.40 CFI Plan Apo VC oil-immersion objective. Images were analyzed using NIS-Elements microscope imaging software.

Animal procedures

Animal procedures were carried out in accordance with the Institutional Animal Care and Use Committee-approved protocol at the Biological Resource Centre, Singapore. Mice were kept at room temperature with a 12 h light-dark cycle and had free access to food and water. Saline or β3-adrenergic receptor agonist CL-316,243 compound (1 mg/kg) was intraperitoneally administered daily. BALB/c mice (InVivos) aged 6–8 weeks were anesthetized using 2% isoflurane in O_2. Once anesthesia was fully induced, the animal was shaved with a hair trimmer in the area where the inguinal WAT (iWAT) was located. The shaved area was sterilized with three alternating wipes of Betadine and 70% ethanol. The adipose tissue was held in place with forceps and the rAAV was injected (1.0×10^{10} viral genomes per 20 μl in phosphate-buffered saline) with a 0.3 cc, 31 gauge insulin syringe. The procedure was repeated on the opposite iWAT to complete the bilateral injection.

In vivo and ex vivo fluorescence imaging

Imaging was performed using the Bruker In-Vivo Xtreme imaging system (Bruker, Germany). Fluorescence images were captured with the following parameters: exposure time, 10 s; F/stop, 1.1; excitation filter, 700 nm; emission filter, 750 nm. For anatomical coregistration, reflectance images were acquired with the following parameters: exposure time, 0.1 s; F/stop, 2.8. The data were analyzed with the Bruker Molecular Imaging software.

MSOT imaging and processing

For optoacoustic imaging, an MSOT inVision 512-echo small animal imaging system (iThera Medical GmbH, Munich, Germany) was employed (24). Details of the imaging system can be found in the supplemental Materials and Methods. A volumetric region of interest consisting of multiple transverse slices spanning the whole abdomen with an inter-slice distance of 0.5 mm was initiated from the kidneys to the bladder region. Image reconstruction was achieved with the back-projection algorithm in the proprietary ViewMSOT software suite (ver3.7; iThera Medical). Optoacoustic signals acquired were resolved spatially and quantitatively by spectral unmixing (negative values were discarded) via least-squares linear regression (25) into corresponding individual chromophores (lipid, iRFP720). For convenient visualization, the MSOT lipid and iRFP720 signals were overlaid on the anatomical ultrasound image to display the spatial distribution of the chromophores in the abdomen in pseudo-color (magenta, iRFP720 signal; green, lipid signal). The sample anatomical reference is shown in supplemental Fig. S2. For semi-quantification, the mean optoacoustic signals within the represented region of interest over the lipid and iRFP720 signals in transverse MSOT slices were attained with proprietary ViewMSOT and open-source FIJI software (Image J, National Institutes of Health). Signal intensities measured were then plotted using GraphPad Prism.

PET imaging coupled with MRI

The animals were imaged longitudinally on the Mediso nanoscan 3T MR-PET system using a modified version of the methodology described by Wang, Minze, and Shi (26). Briefly, animals were anesthetized using inhalational isoflurane anesthesia (maintained at 1.5% alveolar concentration) and injected with ^{18}F-FDG (~10 MBq per animal) via the lateral tail vein. They were maintained heated and anesthetized throughout the procedure. Static PET acquisitions were performed at 60–70 min post injection and a multi field of view T1-weighted axial spin echo MR scan was used to delineate fat depots (TR 1,339 ms, TE 10.2 ms, matrix size 256 × 256, 50.0 mm FOV, and 0.7 mm slice thickness with no slice gap acquisition time 12 min). Animals were monitored for maintenance of body temperature and respiration rate during imaging studies using the Biovet physiological monitoring system. Post analysis of reconstructed calibrated images was performed with FIJI and Amide software (version 10.3, Sourceforge). Uptake of radioactivity in the fat depots was determined by placement of a volume of interest around the fat region, as delineated by MR imaging. A volume of interest was also placed in the quadriceps muscle to provide reference tissue values.

Histology

Tissues were dissected and fixed with 10% formalin. Fixed tissues were embedded in paraffin and sectioned. Sections were stained with H&E or were probed with antibody for UCP1 (1:100; ab23841, Abcam). Images were taken using a Nikon TS-100-F microscope.

Statistical analysis

Data are expressed as mean ± SEM. Analyses were performed using Micorsoft Excel or GraphPad Prism. Statistical significance was assessed by two-tailed Student's *t*-test to analyze the difference between two groups. Statistical significance was defined as $P < 0.05$. The correlation between PET and MSOT data points was analyzed by Pearson's correlation, which yielded correlation coefficients and P values.

RESULTS

Development of reporter system for monitoring adipose browning in the optical system

To assess the extent of browning in WAT with optical imaging, we generated a reporter construct in which expression of iRFP720 is driven by a short version of the UCP1 (mini/UCP1) promoter (27, 28), which was previously shown to contain the minimal regulatory elements required for transcriptional activity (**Fig. 1A**). As a positive control for the iRFP720 activity during in vitro imaging studies, we also generated a DNA construct to express iRFP720 driven by constitutive PGK promoter (Fig. 1A). We first validated the reporter activity upon browning stimulation with FSK treatment, following adipogenesis in 3T3L1 preadipocytes transduced with lentivirus encoding the respective reporter constructs. Expression of iRFP720 was first confirmed by fluorescence microscopy. We observed the iRFP720 signal after FSK treatment in 3T3L1 cells stably expressing mini/UCP1-iRFP720 (Fig. 1B). In addition, protein lysates were harvested from the transduced 3T3L1 cells treated with either FSK or DMSO control. In concordance with our fluorescence microscopy, we observed induction of the iRFP720 signal in FSK-treated cells from both MSOT analysis (Fig. 1C) and optical imaging using the Bruker Xtreme system (Fig. 1D). Furthermore, elevated expression of *Ucp1* and other thermogenic genes, but not of adipogenic genes, was observed in mature adipocytes that stably express iRFP720 reporter upon FSK treatment, indicating that the reporter activation does not perturb the normal browning function of cells (Fig. 1E).

To evaluate the ability of the reporter system to recapitulate induction of Ucp1 expression in WAT during browning, iWAT was administered with rAAV encoding for the mini/UCP1-iRFP720. Following treatment with specific β_3 adrenergic receptor agonist, CL-316,243, an increase in iRFP720 signals was detected in iWAT in response to chronic CL-316,243 treatment compared with the control treatment with both in vivo (**Fig. 2A**, B) and ex vivo imaging (Fig. 2C, D). The browning of iWAT was further evidenced by the presence of multilocular adipocytes in CL-316,243-treated animals (Fig. 2E), suggesting that the UCP1-iRFP720 reporter accurately mimics changes in *Ucp1* elicited during the browning process and thus serves as a useful tool to quantify changes during adipose browning in vivo.

Monitoring the browning process longitudinally by optoacoustic imaging

To further demonstrate that the UCP1 promoter-driven reporter system was capable of visualizing browning noninvasively in vivo, the expression profile of the iRFP720 protein following rAAV injection was monitored via MSOT before and at several time points after adrenergic stimulation. Optoacoustic signals of iRFP720 protein (pseudo-colored in magenta) could be discerned at day 4 and thereafter in mice administered with CL-316,243 (**Fig. 3A**). In contrast, iRFP720 fluorescence activity was not detected in saline-treated animals (Fig. 3B). Time course quantification of the iRFP720 optoacoustic signals in the iWAT for CL-316,243- and saline-treated animals revealed significant induction of iRFP720 expression at day 4 [0.177 ± 0.009 arbitrary units (au)] post adrenergic stimulation with its peak expression achieved at day 7 (0.229 ± 0.020 au) before reaching plateau at day 10 (0.218 ± 0.037 au) (Fig. 3C).

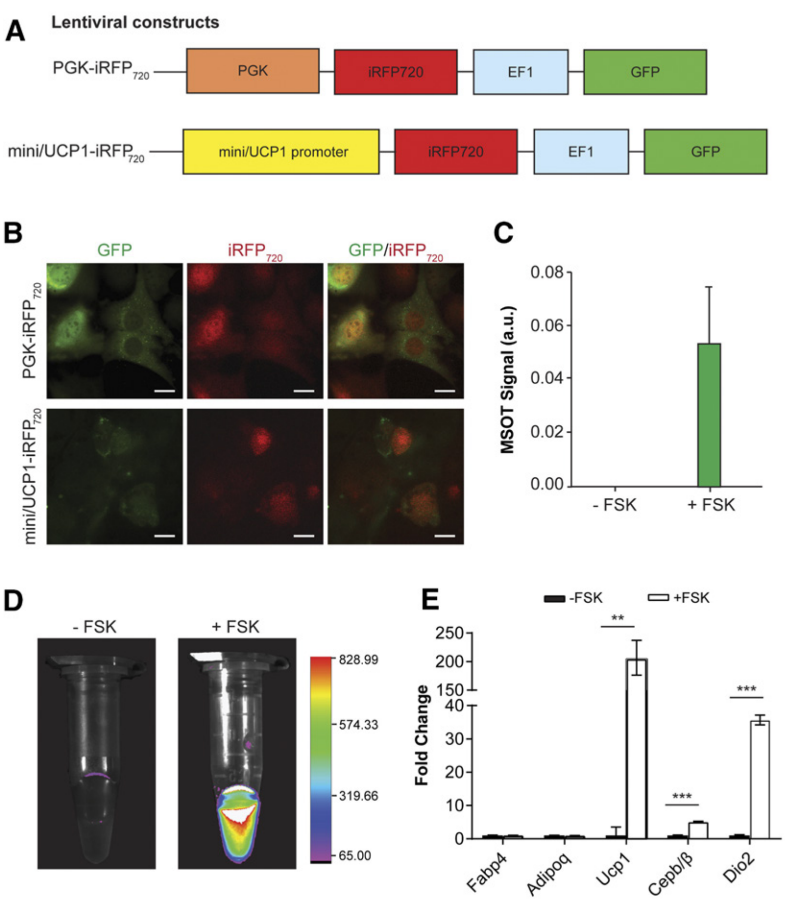

Fig. 1. Validating *Ucp1* reporter system in vitro. A: Lentiviral constructs expressing iRFP720 under the control of a constitutive PGK promoter or an inducible mini/UCP1 promoter. A separate EF1 promoter drives the expression of GFP. B: Representative fluorescence images of 3T3L1 cells infected with PGK-iRFP720 or mini/UCP1-iRFP720 following adipocyte differentiation and browning. The fluorescent signals of the red channel were enhanced to the same degree for presentation purposes. Scale bar, 20 μm. C: MSOT activity of protein lysates from differentiated mini/UCP1-iRFP720 expressing 3T3L1 cells with or without browning by FSK treatment. D: Optical imaging of differentiated 3T3L1 cell lysates with or without FSK using a Bruker Xtreme system. E: Normalized gene expression of adipogenic and thermogenic genes in differentiated 3T3L1 cells with or without FSK treatment. Data are expressed as mean ± SEM. $^{**}P < 0.005$, $^{***}P < 0.001$.

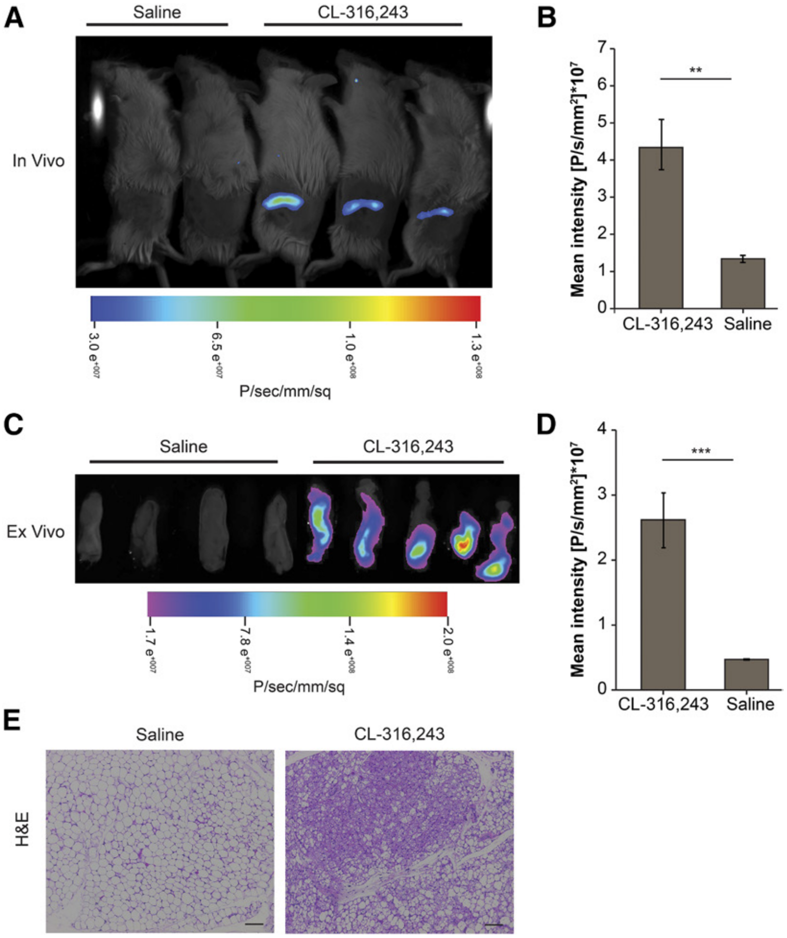

Fig. 2. In vivo validation of the *Ucp1* gene reporter system using a Bruker Xtreme imaging system. A: In vivo iRFP720 activity in mice treated with saline (n = 4) or CL-316,243 (n = 9) for 7 days. Representative mice are shown. B: Quantification of the mean fluorescence intensity of iRFP720 in the iWAT shown in A. C: Ex vivo imaging of representative iWAT excised from the animals in A. D: Quantification of the mean fluorescence intensity of iRFP720 in the iWAT shown in C (n = 4–9). E: H&E sections of iWAT from saline- and CL-316,243-treated mice at day 7. Scale bar, 100 μm. Data are expressed as mean ± SEM. ** $P < 0.01$, *** $P < 0.005$.

Next, we hypothesized that enhanced fatty acid oxidation during browning of WAT might result in attenuated lipid distribution during optoacoustic imaging. To examine this, we took advantage of the spectra absorption of the CH_2 group in lipids, which allows the iWAT to be distinguished from the surrounding tissues by optoacoustic imaging. Notably, the lipid signals (pseudo-colored in green) in iWAT of CL-316,243-treated animals diminished over time during beiging (Fig. 3A, D). On the other hand, the lipid signals of the saline-treated animals were significantly higher than those of the CL-316,243-treated animals at days 4, 7, and 10 (132 ± 2 au vs. 99 ± 9 au, 148 ± 5 au vs. 97 ± 7 au, and 145 ± 4 au vs. 90 ± 5 au, respectively; $P < 0.05$). Furthermore, the reduced lipid signals were observed in close proximity and/or overlapping with optoacoustic iRFP720 activity in the iWAT area (Fig. 3A), suggesting an increase in UCP1-mediated lipid metabolism during iWAT browning. Consistent with the increase in iRFP720 activity, CL-316,243-treated mice showed a marked increase in multi-locular beige adipocytes and robust induction of UCP1 protein in iWAT, as demonstrated by histological and immunoblot analyses (Fig. 3E, F).

Quantification of adipose browning with FDG-PET imaging coupled with MRI

In order to determine whether adipose browning could be monitored and correlated with a clinically translatable system, small animal PET/MR imaging was performed on the same animals following MSOT-US imaging at days 1, 4, 7, and 10 during adrenergic stimulation, as shown in supplemental Fig. S1. As seen in **Fig. 4A**, the retention of ^{18}F-FDG in the iWAT area determined by MRI was significantly increased by treatment with CL-316,243. Adrenergic treatment had no significant effect on iWAT retention of ^{18}F-FDG [1.64 ± 0.82% injected dose (ID)/g] compared with vehicle treatment (1.63 ± 0.53% ID/g) on day 1. The retention of ^{18}F-FDG was significantly increased in the CL-316,243-treated iWAT area by day 4 (3.39 ± 1.35% ID/g vs. 1.87 ± 0.56% ID/g in the vehicle-treated iWAT) and was further increased at day 7 (4.29 ± 0.89% ID/g vs. 1.48 ± 0.41% ID/g). At day 10, the retention of ^{18}F-FDG in the CL-316,243-treated iWAT was still significantly greater than the vehicle-treated iWAT (3.10 ± 1.71% ID/g vs. 1.61 ± 0.57% ID/g). In order to investigate the association between PET/MR and MSOT imaging analyses of browning, the PET data and MSOT data points were paired for each time point and in individual animals for CL-316,243-treated and saline control groups, and were assessed using Pearson's correlation analysis. A Pearson r score of 0.68, $P < 0.0001$ was obtained for the paired PET and MSOT data in iWAT with CL-316,243 treatment, in contrast to $r = -0.13$ (not significant) with the vehicle treatment (Fig. 4B), indicating that the observed changes in optoacoustic iRFP720 signals were strongly correlated with the ^{18}F-FDG signals measured by PET imaging during browning.

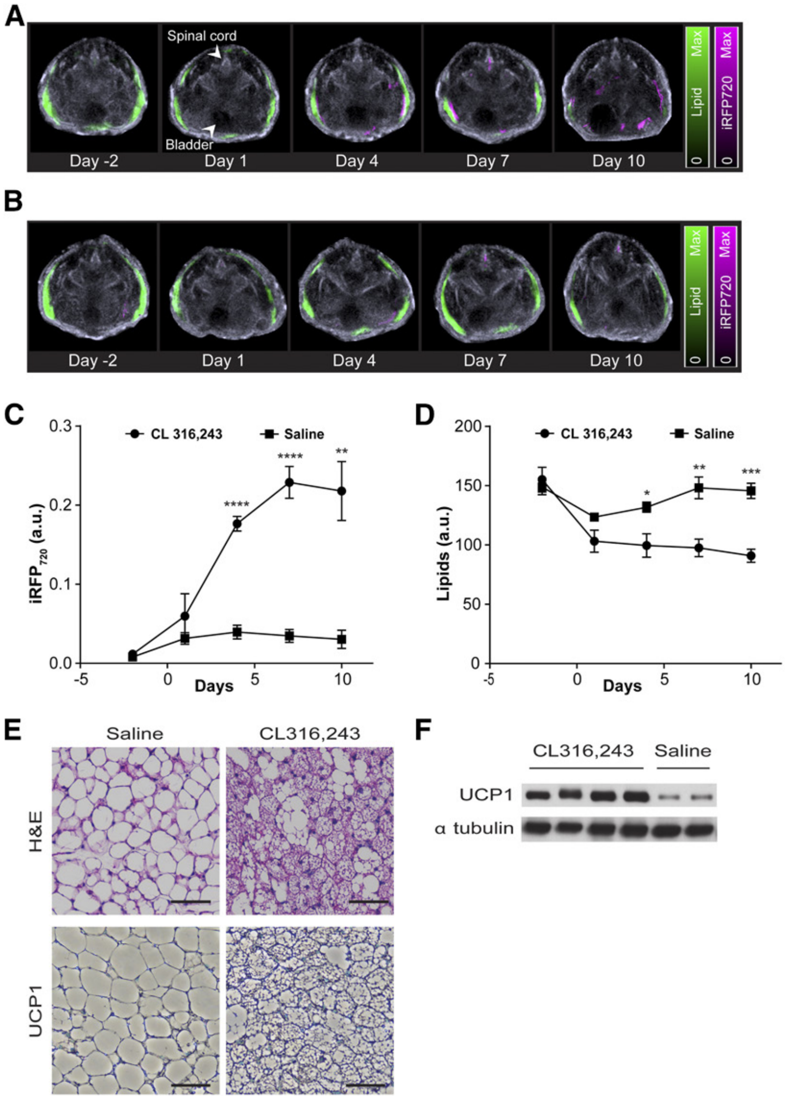

Fig. 3. Real-time imaging of WAT browning with MSOT. Lipid signals (green) and iRFP720 signals (magenta) in the iWAT region of representative mice at various time points with CL-316,243 (A) and saline (B) injections. Lipid and iRFP720 optoacoustic signals were superimposed on ultrasound anatomical images; Optoacoustic signal quantification of iRFP720 (C) and lipids (D) in the iWAT region of CL-316,243-treated (n = 7) and saline-treated (n = 5) mice at various time points post treatment. E: Representative H&E (top panel) and immunohisto-staining for UCP1 (bottom panel) in iWAT sections from saline- and CL-316,243-treated mice. Scale bar, 100 μm. F: Representative immunoblots for UCP1 and α tubulin (loading control) in iWAT lysates that were isolated from saline- and CL-316,243-treated mice. The bands were cropped from different areas and exposures of the same Western blot gel, which is shown in supplemental Fig. S3. Data are expressed as mean ± SEM. *$P < 0.05$, **$P < 0.01$, ***$P < 0.005$, ****$P < 0.001$.

DISCUSSION

The discovery of brown/beige fat in adult humans has rekindled the interest in its role as a regulator of energy homeostasis and excitement over the possibility of activating browning of WAT to enhance energy expenditure for the treatment of obesity and metabolic diseases. The development of new pharmacological agents that augment browning activity necessitates the use of sensitive and specific preclinical imaging methodologies that are well correlated with *Ucp1* expression, which is a marker for browning.

To date, there are a few strategies employed for the development of molecular probes that specifically target BAT. Because BAT is highly vascularized, probes have been developed to exploit this characteristic, including IR786 (a lipophilic cationic near infrared fluorescence dye) and peptide PEP3 (29, 30). Micelles loaded with SRFluor680 and curcumin analogs have also been proposed as alternative molecular probes specific for BAT (31, 32). Although these probes have demonstrated some success in in vivo imaging of BAT, they indirectly target vascular cells rather than brown adipocytes of BAT, and the ability of these probes for real-time monitoring of browning in WAT remains largely unexplored. While this work was in preparation, two studies recently reported that label-free imaging approaches allow for noninvasive and real-time measurement of BAT metabolic activity, by taking advantage of the presence of endogenous chromophores and autofluorescence signals from hemoglobin and intracellular NADH, respectively (33, 34). Of particular interest is the optoacoustic detection of BAT metabolism indirectly by measuring the hemoglobin oxygenation gradient resulting from increased oxygen consumption (34).

Alternative imaging techniques have attempted to assess surrogates of *Ucp1* activation during brown fat activation, whereby the transgenic mouse expresses a luciferase gene under the control of a *Ucp1* promoter (35, 36). However, it takes a longer time and is more costly to generate the transgenic mouse lines, and is restricted to use of imagers compatible with bioluminescence. In contrast to BAT-targeted fluorescent probes and luciferase reporter, we have demonstrated that a near-infrared fluorescent protein, iRFP720 (as a reporter driven by the *Ucp1* gene promoter), is applicable for localization and longitudinal quantitation of

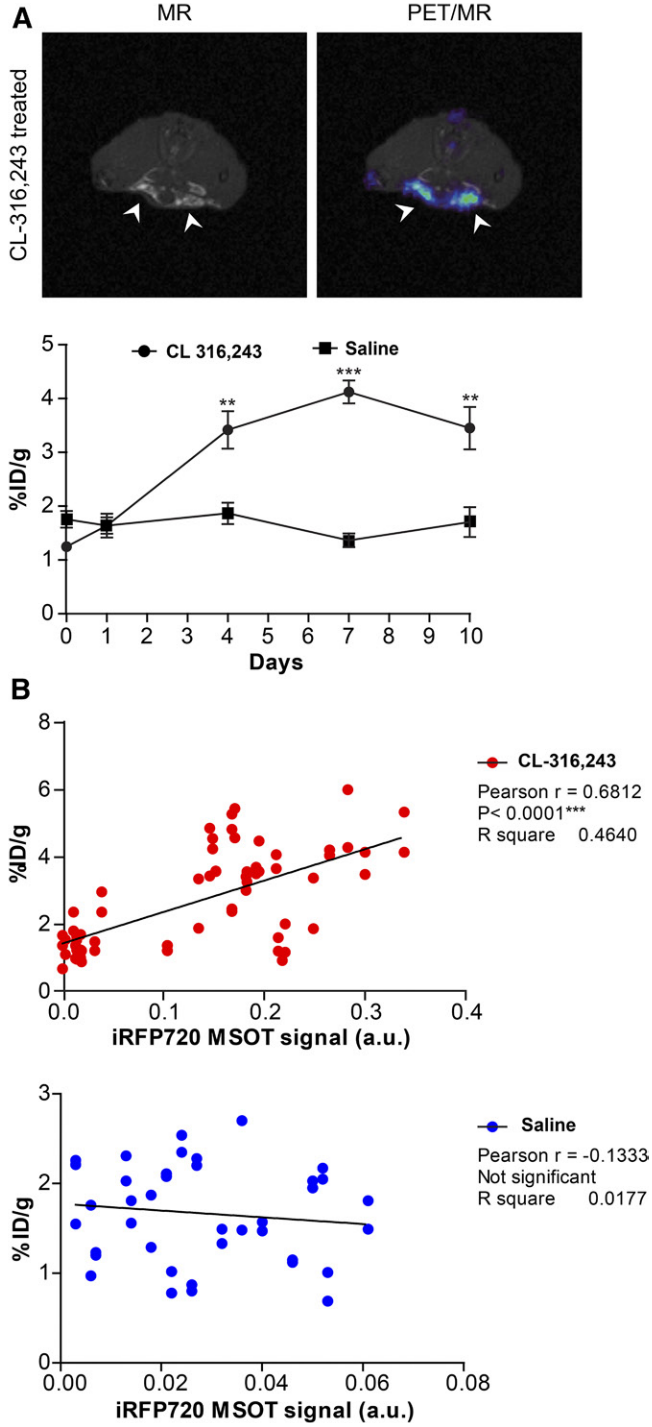

Fig. 4. PET/MR imaging of ^{18}F-FDG during WAT browning. A: Graph showing retention of ^{18}F-FDG measured by longitudinal PET imaging (~10 MBq, acquired from 70 to 90 min post injection under isoflurane anesthesia). Fat depots were delineated by T1-weighted MRI, as indicated by arrowheads. Retention was significantly higher in the iWAT of mice administered with CL-316,243 (n = 7) compared with the saline control (n = 5) at days 4, 7, and 10 post treatment. B: Scatter plots showing the correlation between the iRFP720 activity measured by MSOT and ^{18}F-FDG uptake as determined by PET in the CL-316,243-treated (upper panel) and saline control (lower panel) groups. The iRFP720 activity is shown on the x axis, whereas the ^{18}F-FDG uptake is shown on the y axis. Pearson's correlation coefficient (*r*) is presented. Data are expressed as mean ± SEM. $^{**}P < 0.01$, $^{***}P < 0.001$.

adipose browning in vivo in a real-time manner. By using MSOT-US to image expression of *Ucp1*-based iRFP720 signals, it is possible to achieve higher penetration depth with minimal signal attenuation in tissues, as compared with other optical imaging modalities. Through generating the concentration map of the endogenous lipids and iRFP720 chromophores in the subcutaneous area, MSOT enables estimation of the degree of WAT browning in real time, as well as the accompanying changes in lipid metabolism. Our findings demonstrated an increase in *Ucp1* expression, indicated by an increase in iRFP720 activity showing the presence of functionally active beige fat in iWAT as early as 4 days post stimulation with CL-316,243. Furthermore, WAT browning was also confirmed independently using PET/MR imaging methodology, as evidenced by a robust increase in ^{18}F-FDG uptake during adrenergic stimulation.

It has previously been shown that activation of browning in WAT gives rise to enhanced lipolysis and fatty acid oxidation, which result in hydrolysis of stored triglycerides into free fatty acids and their catabolism (37, 38). Consistent with earlier studies, we observed a gradual attenuation of lipid signals with a concomitant increase in iRFP720 reporter activity over the time course of β_3 adrenergic stimulation in vivo with MSOT-US imaging. The system therefore allows real-time monitoring of dynamic changes in lipid metabolism triggered by browning activation, which offers additional benefit. Though PET/CT imaging with ^{18}F-FDG has been the gold standard imaging modality for assessing BAT in rodents and humans, the uptake of ^{18}F-FDG is an indirect measure of glucose uptake, and it is often difficult to distinguish between BAT and other metabolically active tissues. By combining PET with MRI that can identify fat depots by T1-weighted images, we demonstrated that the system can reliably assess adipose browning levels, which are well correlated with those measured by the optoacoustic system.

In conclusion, we demonstrated the utility of the optical system coupled with a novel reporter and PET/MR system with ^{18}F-FDG for the longitudinal in vivo monitoring of changes in the generation of beige fat depots in WAT. This tool thus offers great potential for the identification and characterization of novel biological mechanisms and therapeutics aimed at modulating adipose browning in vivo.

The authors thank Soo Jian Chow and Benjamin Sim from SBIC-Nikon Imaging Centre, Singapore for their assistance in microscopy imaging and Dr. Nikita Agarwal from SBIC-Bruker Preclinical Imaging Centre, Singapore for guidance and technical assistance on in vivo imaging with the Bruker Xtreme system. The authors also thank members of the Fat Metabolism and Stem Cell Group and the Laboratory of Metabolic Medicine for advice and help in performing the experiments.

REFERENCES

1. Paidisetty, S., and T. M. Blodgett. 2009. Brown fat: atypical locations and appearances encountered in PET/CT. *AJR Am. J. Roentgenol.* **193:** 359–366.
2. Virtanen, K. A., M. E. Lidell, J. Orava, M. Heglind, R. Westergren, T. Niemi, M. Taittonen, J. Laine, N. J. Savisto, S. Enerback, et al. 2009.

Functional brown adipose tissue in healthy adults. *N. Engl. J. Med.* **360:** 1518–1525.

3. Cypess, A. M., S. Lehman, G. Williams, I. Tal, D. Rodman, A. B. Goldfine, F. C. Kuo, E. L. Palmer, Y. H. Tseng, A. Doria, et al. 2009. Identification and importance of brown adipose tissue in adult humans. *N. Engl. J. Med.* **360:** 1509–1517.
4. van Marken Lichtenbelt, W. D., J. W. Vanhommerig, N. M. Smulders, J. M. Drossaerts, G. J. Kemerink, N. D. Bouvy, P. Schrauwen, and G. J. Teule. 2009. Cold-activated brown adipose tissue in healthy men. *N. Engl. J. Med.* **360:** 1500–1508.
5. Nedergaard, J., T. Bengtsson, and B. Cannon. 2007. Unexpected evidence for active brown adipose tissue in adult humans. *Am. J. Physiol. Endocrinol. Metab.* **293:** E444–E452.
6. Saito, M., Y. Okamatsu-Ogura, M. Matsushita, K. Watanabe, T. Yoneshiro, J. Nio-Kobayashi, T. Iwanaga, M. Miyagawa, T. Kameya, K. Nakada, et al. 2009. High incidence of metabolically active brown adipose tissue in healthy adult humans: effects of cold exposure and adiposity. *Diabetes.* **58:** 1526–1531.
7. Bartelt, A., O. T. Bruns, R. Reimer, H. Hohenberg, H. Ittrich, K. Peldschus, M. G. Kaul, U. I. Tromsdorf, H. Weller, C. Waurisch, et al. 2011. Brown adipose tissue activity controls triglyceride clearance. *Nat. Med.* **17:** 200–205.
8. Gunawardana, S. C., and D. W. Piston. 2012. Reversal of type 1 diabetes in mice by brown adipose tissue transplant. *Diabetes.* **61:** 674–682.
9. Cypess, A. M., L. S. Weiner, C. Roberts-Toler, E. Franquet Elia, S. H. Kessler, P. A. Kahn, J. English, K. Chatman, S. A. Trauger, A. Doria, et al. 2015. Activation of human brown adipose tissue by a beta3-adrenergic receptor agonist. *Cell Metab.* **21:** 33–38.
10. Wu, J., P. Bostrom, L. M. Sparks, L. Ye, J. H. Choi, A. H. Giang, M. Khandekar, K. A. Virtanen, P. Nuutila, G. Schaart, et al. 2012. Beige adipocytes are a distinct type of thermogenic fat cell in mouse and human. *Cell.* **150:** 366–376.
11. Guerra, C., R. A. Koza, H. Yamashita, K. Walsh, and L. P. Kozak. 1998. Emergence of brown adipocytes in white fat in mice is under genetic control. Effects on body weight and adiposity. *J. Clin. Invest.* **102:** 412–420.
12. Vitali, A., I. Murano, M. C. Zingaretti, A. Frontini, D. Ricquier, and S. Cinti. 2012. The adipose organ of obesity-prone C57BL/6J mice is composed of mixed white and brown adipocytes. *J. Lipid Res.* **53:** 619–629.
13. Barbatelli, G., I. Murano, L. Madsen, Q. Hao, M. Jimenez, K. Kristiansen, J. P. Giacobino, R. De Matteis, and S. Cinti. 2010. The emergence of cold-induced brown adipocytes in mouse white fat depots is determined predominantly by white to brown adipocyte transdifferentiation. *Am. J. Physiol. Endocrinol. Metab.* **298:** E1244–E1253.
14. Himms-Hagen, J., A. Melnyk, M. C. Zingaretti, E. Ceresi, G. Barbatelli, and S. Cinti. 2000. Multilocular fat cells in WAT of CL-316243-treated rats derive directly from white adipocytes. *Am. J. Physiol. Cell Physiol.* **279:** C670–C681.
15. Sharp, L. Z., K. Shinoda, H. Ohno, D. W. Scheel, E. Tomoda, L. Ruiz, H. Hu, L. Wang, Z. Pavlova, V. Gilsanz, et al. 2012. Human BAT possesses molecular signatures that resemble beige/brite cells. *PLoS One.* **7:** e49452.
16. Bhanu Prakash, K. N., S. K. Verma, J. Yaligar, J. Goggi, V. Gopalan, S. S. Lee, X. Tian, S. Sugii, M. K. Leow, K. Bhakoo, et al. 2016. Segmentation and characterization of interscapular brown adipose tissue in rats by multi-parametric magnetic resonance imaging. *MAGMA.* **29:** 277–286.
17. Ntziachristos, V., and D. Razansky. 2010. Molecular imaging by means of multispectral optoacoustic tomography (MSOT). *Chem. Rev.* **110:** 2783–2794.
18. Wang, L. V., and S. Hu. 2012. Photoacoustic tomography: in vivo imaging from organelles to organs. *Science.* **335:** 1458–1462.
19. Shcherbakova, D. M., and V. V. Verkhusha. 2013. Near-infrared fluorescent proteins for multicolor in vivo imaging. *Nat. Methods.* **10:** 751–754.
20. Brunker, J., J. Yao, J. Laufer, and S. E. Bohndiek. 2017. Photoacoustic imaging using genetically encoded reporters: a review. *J. Biomed. Opt.* **22:** 070901.
21. Deliolanis, N. C., A. Ale, S. Morscher, N. C. Burton, K. Schaefer, K. Radrich, D. Razansky, and V. Ntziachristos. 2014. Deep-tissue reporter-gene imaging with fluorescence and optoacoustic tomography: a performance overview. *Mol. Imaging Biol.* **16:** 652–660.
22. Qin, C., K. Cheng, K. Chen, X. Hu, Y. Liu, X. Lan, Y. Zhang, H. Liu, Y. Xu, L. Bu, et al. 2013. Tyrosinase as a multifunctional reporter gene for photoacoustic/MRI/PET triple modality molecular imaging. *Sci. Rep.* **3:** 1490.
23. Guo, P., Y. El-Gohary, K. Prasadan, C. Shiota, X. Xiao, J. Wiersch, J. Paredes, S. Tulachan, and G. K. Gittes. 2012. Rapid and simplified purification of recombinant adeno-associated virus. *J. Virol. Methods.* **183:** 139–146.
24. Morscher, S., W. H. Driessen, J. Claussen, and N. C. Burton. 2014. Semi-quantitative Multispectral Optoacoustic Tomography (MSOT) for volumetric PK imaging of gastric emptying. *Photoacoustics.* **2:** 103–110.
25. Tzoumas, S., N. C. Deliolanis, S. Morscher, and V. Ntziachristos. 2014. Unmixing molecular agents from absorbing tissue in multispectral optoacoustic tomography. *IEEE Trans. Med. Imaging.* **33:** 48–60.
26. Wang, X., L. J. Minze, and Z. Z. Shi. 2012. Functional imaging of brown fat in mice with 18F-FDG micro-PET/CT. *J. Vis. Exp.* doi:10.3791/4060.
27. Cassard-Doulcier, A. M., C. Gelly, F. Bouillaud, and D. Ricquier. 1998. A 211-bp enhancer of the rat uncoupling protein-1 (UCP-1) gene controls specific and regulated expression in brown adipose tissue. *Biochem. J.* **333:** 243–246.
28. Larose, M., A. M. Cassard-Doulcier, C. Fleury, F. Serra, O. Champigny, F. Bouillaud, and D. Ricquier. 1996. Essential cis-acting elements in rat uncoupling protein gene are in an enhancer containing a complex retinoic acid response domain. *J. Biol. Chem.* **271:** 31533–31542.
29. Nakayama, A., A. C. Bianco, C. Y. Zhang, B. B. Lowell, and J. V. Frangioni. 2003. Quantitation of brown adipose tissue perfusion in transgenic mice using near-infrared fluorescence imaging. *Mol. Imaging.* **2:** 37–49.
30. Azhdarinia, A., A. C. Daquinag, C. Tseng, S. C. Ghosh, P. Ghosh, F. Amaya-Manzanares, E. Sevick-Muraca, and M. G. Kolonin. 2013. A peptide probe for targeted brown adipose tissue imaging. *Nat. Commun.* **4:** 2472.
31. Rice, D. R., A. G. White, W. M. Leevy, and B. D. Smith. 2015. Fluorescence imaging of interscapular brown adipose tissue in living mice. *J. Mater. Chem. B Mater. Biol. Med.* **3:** 1979–1989.
32. Zhang, X., Y. Tian, H. Zhang, A. Kavishwar, M. Lynes, A. L. Brownell, H. Sun, Y. H. Tseng, A. Moore, and C. Ran. 2015. Curcumin analogues as selective fluorescence imaging probes for brown adipose tissue and monitoring browning. *Sci. Rep.* **5:** 13116.
33. He, S., Y. An, X. Li, X. Wei, Q. Sun, Z. Wu, and J. Y. Qu. 2018. In vivo metabolic imaging and monitoring of brown and beige fat. *J. Biophotonics.* In press.
34. Reber, J., M. Willershauser, A. Karlas, K. Paul-Yuan, G. Diot, D. Franz, T. Fromme, S. V. Ovsepian, N. Beziere, E. Dubikovskaya, et al. 2018. Non-invasive measurement of brown fat metabolism based on optoacoustic imaging of hemoglobin gradients. *Cell Metab.* **27:** 689–701.e4.
35. Galmozzi, A., S. B. Sonne, S. Altshuler-Keylin, Y. Hasegawa, K. Shinoda, I. H. Luijten, J. W. Chang, L. Z. Sharp, B. F. Cravatt, E. Saez, et al. 2014. ThermoMouse: an in vivo model to identify modulators of UCP1 expression in brown adipose tissue. *Cell Reports.* **9:** 1584–1593.
36. Mao, L., B. Nie, T. Nie, X. Hui, X. Gao, X. Lin, X. Liu, Y. Xu, X. Tang, R. Yuan, et al. 2017. Visualization and quantification of browning using a Ucp1-2A-luciferase knock-in mouse model. *Diabetes.* **66:** 407–417.
37. Granneman, J. G., and H. P. Moore. 2008. Location, location: protein trafficking and lipolysis in adipocytes. *Trends Endocrinol. Metab.* **19:** 3–9.
38. Langin, D., D. Ekholm, M. Ridderstrale, M. Lafontan, and P. Belfrage. 1992. cAMP-dependent protein kinase activation mediated by beta 3-adrenergic receptors parallels lipolysis in rat adipocytes. *Biochim. Biophys. Acta.* **1135:** 349–352.